



JAAS

**Enabling orders of magnitude sensitivity improvement for quantification of Ga in a Ce matrix with a compact Echelle spectrometer**

Journal:	<i>Journal of Analytical Atomic Spectrometry</i>
Manuscript ID	JA-TEC-05-2022-000179.R1
Article Type:	Technical Note
Date Submitted by the Author:	25-Aug-2022
Complete List of Authors:	Rao, Ashwin; Air Force Research Laboratory Space Vehicles Directorate Jenkins, Phillip; Air Force Institute of Technology, Auxier, John; Los Alamos National Laboratory, Actinide Analytical Chemistry Shattan, Michael; National Nuclear Security Administration, Office of Defense Nuclear Nonproliferation Patnaik, Anil; Air Force Institute of Technology, Department of Engineering Physics

SCHOLARONE™  
Manuscripts

# Journal Name

## ARTICLE TYPE

Cite this: DOI: 00.0000/xxxxxxxxxx

## Enabling orders of magnitude sensitivity improvement for quantification of Ga in a Ce matrix with a compact Echelle spectrometer

Ashwin P. Rao,<sup>\*a</sup> Phillip R. Jenkins,<sup>b</sup> John D. Auxier II,<sup>c</sup> Michael B. Shattan,<sup>d</sup> and Anil K. Patnaik<sup>b</sup>

Received Date  
Accepted Date

DOI: 00.0000/xxxxxxxxxx

Chemical analysis of lanthanide materials *via* laser-induced breakdown spectroscopy (LIBS) is often hindered by the complex spectral response and self-absorption phenomena that occur in the LIBS plasma. Previous attempts to quantify the alloying metal gallium in cerium matrices with a handheld LIBS analyzer were plagued by the inability to resolve major Ga atomic emissions and self-absorption effects, diminishing the fidelity of calibration curves. However, implementing a compact, high resolution Echelle spectrometer coupled with a Stark-broadening based self-absorption correction can enable proper recording of the main Ga I emission at 417.2 nm and improve the sensitivity of calibration curves by two orders of magnitude compared to the handheld device. We demonstrate this by using the mathematical correction on recorded high-resolution spectra from Ce-Ga samples to achieve calibration curves with detection limits as low as 0.008 wt% Ga. This study indicates that using a compact spectrometer capable of higher resolution measurements can yield higher fidelity solutions for Pu chemical analysis *via* LIBS in constrained environments, e.g., in a glovebox – enabling higher sensitivity in rapid detection of minor elements.

### 1 Introduction

Laser-induced breakdown spectroscopy (LIBS) is a well-established, versatile analytical technique for elemental determination<sup>1</sup> with applications in a broad range of quantitative analyses such as combustion diagnostics,<sup>2-4</sup> food science,<sup>5</sup> pharmaceutical chemistry,<sup>6</sup> nuclear forensics,<sup>7</sup> metallurgy,<sup>8</sup> and geochemical analysis<sup>9-11</sup>. One particular field where LIBS techniques have garnered significant interest is in the analysis of nuclear materials<sup>12-14</sup>. Specifically, recent studies have investigated LIBS for analysis of alloying elements or impurities in plutonium and plutonium surrogate material<sup>15-17</sup>. This relatively newer application of LIBS seeks to develop predictive models from the complex plutonium spectra relating variations in the intensity of different emission lines to the concentrations of minor elements present in Pu alloys. Developing precise and sensitive calibration models to accomplish this type of analysis would greatly reduce the time require to quality check Pu alloys and bolster Pu component production efforts.

The complex Pu matrix and the resulting complex spectra pose several challenges to conducting accurate quantitative analysis *via* LIBS in such materials. Firstly, the radiation and pyrophoricity hazards posed by Pu metal requires any analysis to be conducted in an argon controlled glovebox<sup>18</sup>; this has generated the need for compact analytical hardware which can be used in such constrained environments. Previous studies implemented a commercially-produced handheld LIBS device for spectral analysis of Pu or Pu surrogates, as the compact analyzer could be wielded by an operator within the limited space of a glovebox<sup>15,17,19</sup>. While the handheld device is effective in the constrained environment, higher-fidelity analysis could be conducted by implementing a compact, high-resolution spectrograph to record LIBS emissions. Another challenge to Pu alloy analysis stems from a measurement issue originating from a phenomenon known as self absorption.

An ideal low-density plasma would be optically thin and thermally homogeneous; meaning light emitted from the plasma centroid can travel through the bulk of the plasma to the detector without being absorbed by colder atoms<sup>20</sup>. Typical LIBS plasmas are both optically thick and thermally inhomogeneous<sup>21</sup>, even for gas-phase LIBS when the gas density is elevated to a few bars<sup>22,23</sup>; plasma emissions tied to the ground state are preferentially absorbed by colder periphery atoms after they are emitted from the plasma center<sup>24,25</sup>. Additionally, higher analyte con-

\* Corresponding Author

<sup>a</sup> Space Vehicles Directorate, Air Force Research Laboratory, Albuquerque, NM 87117

<sup>b</sup> Air Force Institute of Technology, 2950 Hobson Way, WPAFB, OH 45424

<sup>c</sup> Actinide Analytical Chemistry, Chemistry Division, Los Alamos National Laboratory, Los Alamos, NM 87545

<sup>d</sup> Office of Defense Nuclear Nonproliferation, National Nuclear Security Administration, Washington, D.C. 20024

centrations in the bulk material increase optical thickness of the plasma by increasing the population of colder atoms in the periphery to absorb atomic emissions from the analyte being observed<sup>26–28</sup>. Reabsorption of emission photons affects the intensity and shape of emitted wavelength peaks, depending on the degree of optical thickness<sup>29</sup>. This directly detracts the fidelity of calibration curves being built with the affected emission wavelengths, and corrective models need to be developed to reduce these effects in order to improve calibration precision and sensitivity.

A well documented model to correct calibration curves for self-absorption uses the Stark broadening of the self-absorbed lines employing Stark impact parameters to formulate an intensity correction factor which linearizes the calibration curves<sup>26,29–34</sup>. The results of these prior studies definitively demonstrate how the correction method can improve recorded emission peak data to increase the fidelity of calculated plasma diagnostics or calibration curves built with the corrected spectra. In a recent study, this correction method was implemented to minor Ga I emissions in order to correct calibrations for quantifying Ga in Ce matrices<sup>35</sup>, where the aforementioned SciAps Z300 handheld analyzer was used to record the spectra. Because of the limited resolving power of the device ( $R_{avg} = 1300$ ), the major Ga I emission at 417.2 nm could not be properly resolved; hence, the minor emission peaks had to be used for the calibrations.  $R_{avg}$  is defined by the ratio  $\frac{\lambda}{\Delta\lambda}$ ;  $\lambda$  refers to a particular wavelength and  $\Delta\lambda$  is the smallest difference in wavelengths distinguishable at  $\lambda$ . Even with implementation of the self-absorption correction to the calibration curves, the lowest limit of detection (LoD) achievable using this device was only on the order of 0.1 wt% Ga.

This study seeks to improve the performance of calibrations for quantifying Ga by implementing a compact, high resolution spectrograph as an alternative to the handheld LIBS device for recording Ce-Ga emissions. The alternative experimental setup is demonstrated to be capable of yielding higher-resolution *in-situ* Pu alloy analysis, which could potentially improve precision and sensitivity of calibration models for quantifying Ga. This technical note presents the results of using a high-resolution Echelle spectrometer ( $R_{avg} = 7600$ ) with the aforementioned self-absorption correction to improve the fidelity of Ga calibration curves.

## 2 Experimental

### 2.1 LIBS system

Fig. 1 shows the diagram of the laboratory LIBS setup used in this study. To generate the laser-induced plasma, an Everbright 1064 nm Nd:YAG laser operating at an energy of 100 mJ/pulse, pulse width of 10 ns and repetition rate of 10 Hz was used. Using a digital delay generator, a 190 ns delay between the laser flash lamp and Q-switch was set. The beam was directed into a sample chamber and focused onto the sample using a  $f=+30mm$  plano-convex lens to generate an ablation in open air. The delay generator was used to run the laser in burst mode, firing 20 pulses per run 3.5 seconds apart. The sample was shifted every 5 pulses to ablate a different surface location in order to prevent tunneling. Optical emissions from the microplasma were collected with an

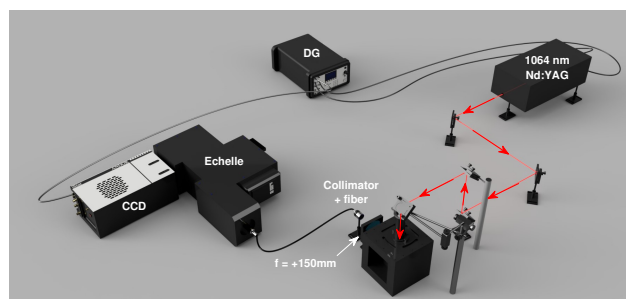


Fig. 1 Experimental LIBS system with 1064 nm Nd:YAG, optical collection hardware, Echelle spectrometer, and CCD camera.

other  $f=+150mm$  plano-convex lens and a ThorLabs F810SMA-543 collimating lens attached to an optical fiber, directing the light into a Catalina Scientific EMU 120/65 Echelle spectrograph. The Echelle had a slit dimension of  $30 \times 120 \mu\text{m}$  with a grating blazed at 505 nm, providing a broadband spectra from 325 to 925 nm at  $\Delta\lambda = 0.01$  nm. The spectra were recorded on an Andor USB iStar CCD camera with a  $1024 \times 1024$  pixel array ( $13 \mu\text{m}$  pixel width) with a gate width of 6  $\mu\text{s}$  and MCP gain of 2000.

### 2.2 Sample creation

The cerium pellet samples were prepared from Sigma Aldrich cerium oxide (99.995%  $\text{CeO}_2$ ) mixed with varying weight percent concentrations of gallium oxide (99%  $\text{Ga}_2\text{O}_3$ ). The powders were milled using an agate mortar and pestle, weighed to achieve the desired weight percent concentrations and then homogenized using a Fluxana MUK mixer. No binding agent was implemented in this study. The mixed powder was then pressed using a 14 mm stainless steel die at 5 metric tons for 120 seconds. Pellets with 0, 0.25, 0.5, 1, 1.5, 2, 2.5, 3 and 5 wt% Ga were created for use in this experiment; the press equipment was cleaned and dried between the creation of each sample pellet to prevent cross-contamination.

## 3 Results and Discussion

### 3.1 Initial line extraction and gate delay variation

Initially, data was collected for 20 spectra of each of the 9 samples at a 500 ns gate delay. It was found from the initial investigation that the major Ga I emission at 417.2 nm present in all spectra from samples containing Ga. In the Fig. 2, the recording of the same Ce-Ga sample are taken with the handheld LIBS and the Echelle setup. Clearly, the signal from the two have visible differences; both cases had the same fundamental laser wavelength, gate delay of 250 ns and repetition rate were used in both measurements. However, it should be noted that the Z300 was fixed at a laser energy of 5 mJ/pulse and a spot size of  $50 \mu\text{m}$ , while the laboratory setup was run at a laser energy of 100 mJ/pulse with a beam spot size approximately  $6.4 \mu\text{m}$ . While the laser parameters between the two methods differ, the major differences in the recorded spectra stem from the different spectrograph resolutions, as illustrated in Fig. 3. The major Ga I emission at

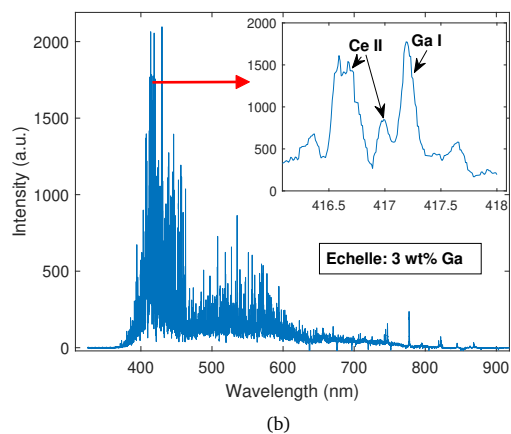
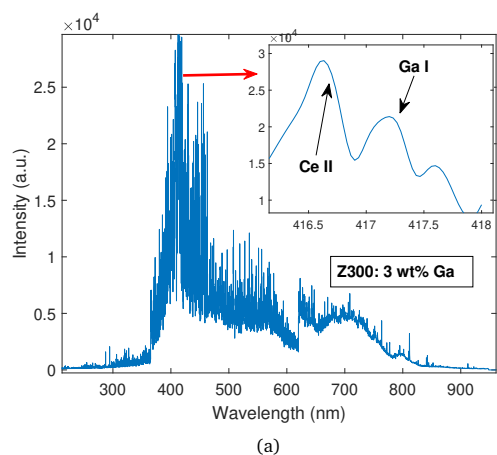


Fig. 2 Comparison of Ga I 417 nm line resolution between a) Z300 and b) Echelle recorded spectra.

417 nm is not well separated in the Z300 spectrum, and there is significant overlap with the neighboring Ce peak. In comparison, the same line is much more visible in the spectrum taken with the Echelle, and is more clearly separated from neighboring emissions. This allowed for the extraction of the full peak from the Echelle spectra for quantitative analysis, highlighting the benefits of using a spectrograph with a higher resolving power for this complex lanthanide matrix.

The LIBS measurements were repeated on the samples at gate delays of 250 and 1000 ns to evaluate temporal changes of the Ga I 417 nm line. Fig. 3 illustrates the relationship between emission line intensity and Ga concentration for 5 of the 9 samples at the shortest and longest delays; each individual peak is an average from 20 spectra and pre-processed using background subtraction and a filtering method<sup>36,37</sup>. The full 417 nm emission is easily extractable without interference from the nearby Ce II emission, unlike in the handheld LIBS spectra, allowing for easy pre-processing for quantitative analysis. While the intensity follows the expected trend of increasing with Ga content at each gate delay, the behavior at 250 ns differs significantly from the 1000 ns recordings. At 250 ns it would appear that the increase in intensity begins to fall off as the Ga content approaches 5 wt%, with the overall trend being distinctly nonlinear. This effect is

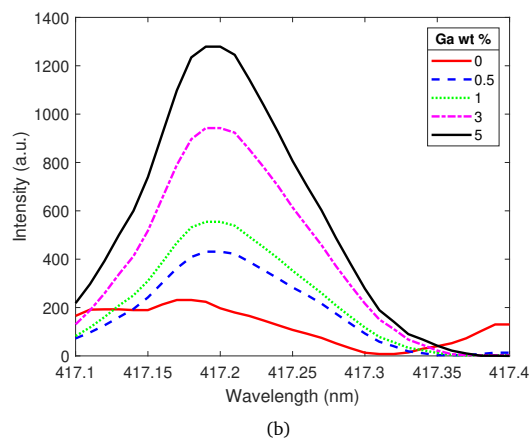
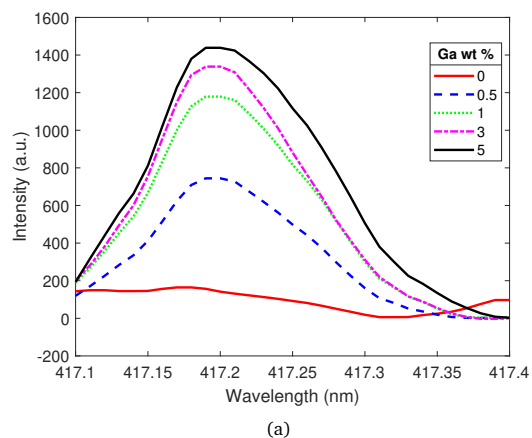


Fig. 3 Ga I 417.2 nm line intensity relationship to Ga concentration at (a) 250 ns (b) 1000 ns gate delay, showing a non-linear intensity increases as Ga content increases in the samples.

much less pronounced at 1000 ns. This initial visual inspection of the emission lines points to the presence of self-absorption suppressing intensity increases at higher concentrations, particularly at early gate delay times.

Calibration curves relating the peak intensity of the Ga I 417 nm line to the Ga concentration were built for all three gate delay times. The 20 recordings taken for one sample at a given gate delay time were averaged; intensity of the Ga line was extracted from this averaged spectra, and uncertainty was calculated as the standard deviation of mean peak intensity measurement at each Ga concentration as determined by established error propagation rules<sup>38</sup>. To quantitatively evaluate self-absorption, a power curve in the form of Eq. 1 was fit to the data to yield a calibration curve. Calibration curves of this form have been used in previous LIBS experiments to evaluate self-absorption behavior<sup>39-41</sup>. This provided a relationship between the peak intensity ( $I$ ) at each concentration ( $C$ ), which varied based on an intercept factor ( $a$ ) and an exponent ( $b$ ) known as the self-absorption (SA) coefficient. A curve with  $b \approx 1$  denotes no self-absorption, and smaller values of  $b$  indicate the greater effect of the phenomenon on the spectral intensity.

$$I = aC^b \quad (1)$$

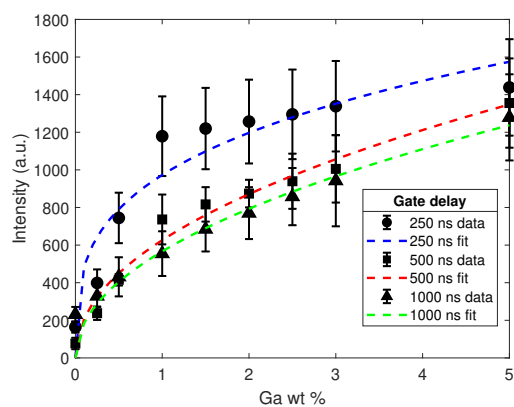


Fig. 4 Calibration curves using Ga 417 nm peak intensity at 250, 500 and 1000 ns gate delay, showing the effects of self-absorption on the peak intensity affecting the shape of the calibration fits.

The corresponding power fits to the peak intensity data at each gate delay time are illustrated in Fig. 4; the data demonstrates the presence of self-absorption in the plasma causing the calibration curves to deviate significantly from a linear form. The fitting parameters for each data set are listed in Table 1. A visual in-

Table 1 Calibration curve regression (*a*) and SA (*b*) coefficients at each gate delay time ( $t_d$ ) for the curves in Fig. 4.

$t_d$ (ns)	a	b
250	972.9	0.2992
500	626.0	0.4764
1000	566.4	0.4855

spection of each calibration curve concludes that self-absorption has a greater effect on the calibration at an earlier gate delay, as the 250 ns curve shows a more pronounced 'elbow' where the curve deviates from linear behavior. However, collecting the spectra at later times reduces recorded signal intensity as the LIBS plasma is significantly cooler, which diminishes the sensitivity of a derived calibration curve<sup>42</sup>. Thus, there is a trade-off between the mitigation of self-absorption effects and achievable univariate calibration sensitivity when increasing the gate delay. This trend is expressed in the fitting parameters shown in table 1 as longer gate delays yield a lower 'a' coefficient (sensitivity) while improving the 'b' coefficient (self absorption). One should also note that continuing to extend the gate delay leads to diminishing improvements in self absorption after about 500 ns while sensitivity continues to decrease at faster rate. This behavior indicates that extending the gate delay can only partially mitigate the effects of self-absorption, as the increases in linearity will plateau while the loss of total signal persists.

### 3.2 Self-absorption correction results and analysis

The previously discussed mathematical self-absorption correction was implemented on the Ga I 417 nm peaks recorded with the Echelle. The Stark FWHM was extracted from each recorded Ga peak using a Voigt profile fitting routine<sup>43</sup>. Eq. 2 relates the measured peak FWHM ( $\Delta\lambda$ ), Stark FWHM ( $w_s$ ) and electron density

( $n_e$ ) to the ratio of the measured ( $I$ ) and non self-absorbed ( $I_0$ ) intensity, which is represented as the correction factor SA. The exponent  $\beta$  is given as -0.54. This formula is derived from the established equation for Stark broadening in literature<sup>44</sup> and has been used in several previous studies<sup>28,31,34,45</sup>.

$$SA = \frac{I(\lambda)}{I_0(\lambda_0)} = \left( \frac{\Delta\lambda}{2w_s} \frac{10^{16}}{n_e} \right)^{\frac{1}{\beta}} \quad (2)$$

The SA value was calculated for each recorded peak at each gate delay; the recorded intensities of each peak were subsequently divided by their corresponding SA value to calculate the corrected intensity. Fig. 5 displays the corrected (blue) and uncorrected (red) calibration curves; a visual comparison indicates significantly improved linearity after the application of the corrective methodology.

To evaluate the corrected and uncorrected calibrations, the mean absolute percent error (*MAPE*) and limit of detection (LoD) are calculated as measures of model precision and sensitivity, respectively. *MAPE* is an established statistical measure of regression quality given by Eq. 3, and represents the average error between the actual value ( $y_i$ ) and calibration prediction ( $\hat{y}_i$ ) at each concentration<sup>46</sup>. This gives a percentage error by which the precision of the model can be judged.

$$MAPE = \frac{100}{n} \sum_{i=1}^n \left| \frac{y_i - \hat{y}_i}{y_i} \right| \quad (3)$$

The LoD is defined as the theoretical lowest quantity of analyte in the sample that must be present for the calibration model to reliably quantify analyte presence with 99% accuracy<sup>47</sup>. This is given by the relation in Eq. 4, where  $\sigma$  is the standard deviation of a blank sample in the wavelength region of interest, and  $s$  is the slope of the linear fit to the data. Therefore, the LoD is inversely related to the sensitivity (slope) of the calibration; a higher slope yields a lower LoD and a more sensitive calibration model.

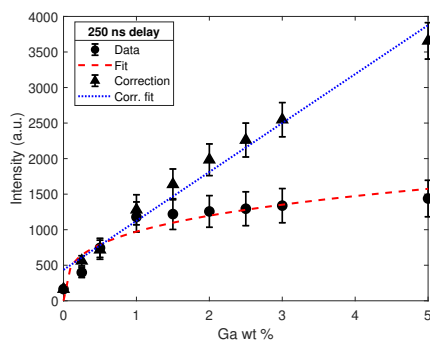
$$LoD = \frac{3\sigma}{s} \quad (4)$$

Table 2 lists these calculated parameters for each gate delay time; *MAPE* was calculated for both corrected and uncorrected calibrations to examine how the mathematical correction affects precision. The mathematical correction greatly reduced the error of all

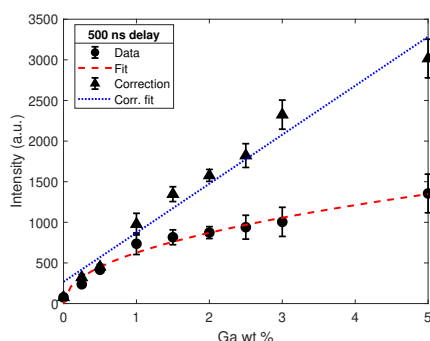
Table 2 Percent error of calibration before and after SA correction, and LoD of the corrected linear calibration model at each gate delay ( $t_d$ ).

$t_d$ (ns)	Uncorr. MAPE	Corr. MAPE	LoD
250	23.5%	7.56%	0.008%
500	19.5%	13.6%	0.009%
1000	14.8%	4.31%	0.015%

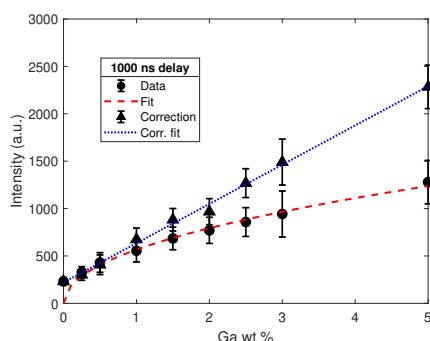
three models up to one order of magnitude; the 1000 ns calibration was the most accurate with a *MAPE* of 4.3%. These results directly parallel those from the previous study using a handheld LIBS device, which saw an order of magnitude reduction in error to the low single percents with the implementation of the SA correction. These results suggest a significant gain in calibration



(a)



(b)



(c)

Fig. 5 Self-absorption corrections of Ga calibration curves at a) 250 ns b) 500 ns and c) 1000 ns

accuracy can be achieved by implementing the correction to linearize the calibration curve.

The sensitivity of the corrected model, evaluated by the LoD, appears to follow the opposing trend as gate delay is increased. Due to the lower intensities recorded at longer gate delays, the slope of the corrected calibration decreases as delay is increased. This in turn increases the LoD of the corrected model, rendering the calibrations less sensitive as  $t_d$  is raised. The 250 ns calibration is most sensitive with an LoD of 80 parts-per-million (ppm), or 0.008 wt% Ga. The 500 and 1000 ns fits yield LoDs of 90 and 150 ppm Ga, respectively. Reaching sub 100s of ppm sensitivity levels for minor metals in a lanthanide or actinide matrix is often difficult with LIBS data due to combined effects of self-absorption and other chemical matrix effects. These results show a two orders of magnitude reduction of detection limits compared to the similar study using a handheld LIBS device, where the lowest LoD achieved was a tenth of a percent Ga in the Ce matrix. The key factor enabling this gain in sensitivity is likely the implementation of the high resolution Echelle spectrograph, which allowed for the proper extraction of the Ga I 417.2 nm line free from neighboring Ce emission interferences. Using a well-resolved, major emission for analysis likely improved the accuracy of the extracted Stark FWHM measurements compared to those taken from the smaller Ga I 287 and 294 nm emissions, leading to an improved intensity correction and higher calibration slope, thereby decreasing the LoD to sub-tenths of a percent levels. While handheld LIBS devices are versatile and easy to use in constrained environments, their limited resolution in turn limits the fidelity of calibrations derived from their spectral recordings. Implementing an alternate LIBS setup leveraging a high-resolution, compact spectrometer can provide the solution needed for yielding high-sensitivity calibration curves for chemical analysis.

## 4 Conclusions

We report a two order of magnitude improvement in sensitivity for quantifying Ga in a Ce matrix with the implementation of a compact, high-resolution Echelle spectrometer. Previous calibration curves derived with LIBS spectra from a handheld LIBS analyzer were unable to reach detection limits below 0.1 wt% Ga, even after the use of a self-absorption correction. The Echelle was able to properly resolve the 417.2 nm Ga I emission, which the handheld LIBS device was unable to do. The corrected calibrations derived from the 417 nm peak data showed detection limits as low as 0.008% Ga, providing a significant gain in sensitivity over previous LIBS calibrations derived from data taken with the handheld device. Since the Echelle is a compact spectrometer, it could be feasible to implement it in constrained environments such as a glovebox in tandem with an external laser source. This would yield a major improvement in capabilities for high-fidelity, *in situ* chemical analysis of plutonium alloys.

## Conflicts of interest

There are no conflicts to declare.

## Acknowledgements

The authors thank Viswa Ramesh for his 3D renders of the experimental setup. This research was supported by funding from the Defense Threat Reduction Agency Nuclear Science and Engineering Research Center as well as the Air Force Office of Scientific Research. This work is approved for public release under 88ABW-2022-0238.

## Notes and references

- 1 D. Hahn and N. Omenetto, *Applied Spectroscopy*, 2010, **64**, 335–66.
- 2 P. S. Hsu, M. Gragston, Y. Wu, Z. Zhang, A. K. Patnaik, J. Kiefer, S. Roy and J. R. Gord, *Appl. Opt.*, 2016, **55**, 8042–8048.
- 3 Y. Wu, M. Gragston, Z. Zhang, P. S. Hsu, N. Jiang, A. K. Patnaik, S. Roy and J. R. Gord, *Combustion and Flame*, 2018, **198**, 120 – 129.
- 4 M. Gragston, P. Hsu, A. Patnaik, Z. Zhang and S. Roy, *Applied Spectroscopy*, 2020, **74**, 340–346.
- 5 E. Bellou, N. Gyftokostas, D. Stefanis, O. Gazeli and S. Couris, *Spectrochimica Acta Part B: Atomic Spectroscopy*, 2020, **163**, 105746.
- 6 P. K. Tiwari, S. Awasthi, R. Kumar, R. K. Anand, P. K. Rai and A. K. Rai, *Lasers in Medical Science*, 2018, **33**, 263–270.
- 7 J. Sirven, A. Pailloux, Y. Baye, N. Coulon, T. Alpettaz and S. Gosse, *J. Anal. At. Spectrom.*, 2009, **24**, 451–459.
- 8 X. Li, Z. Wang, S.-L. Lui, Y. Fu, Z. Li, J. Liu and W. Ni, *Spectrochimica Acta Part B: Atomic Spectroscopy*, 2013, **88**, 180 – 185.
- 9 S. M. Clegg, E. Sklute, M. D. Dyar, J. E. Barefield and R. C. Wiens, *Spectrochimica Acta Part B: Atomic Spectroscopy*, 2009, **64**, 79 – 88.
- 10 R. B. Anderson, J. F. Bell, R. C. Wiens, R. V. Morris and S. M. Clegg, *Spectrochimica Acta Part B: Atomic Spectroscopy*, 2012, **70**, 24 – 32.
- 11 E. C. Ferreira, D. M. Milori, E. J. Ferreira, R. M. Da Silva and L. Martin-Neto, *Spectrochimica Acta Part B: Atomic Spectroscopy*, 2008, **63**, 1216 – 1220.
- 12 B. Bhatt, K. Hudson Angeyo and A. Dehayem-Kamadjeu, *Anal. Methods*, 2018, **10**, 791–798.
- 13 S. Harilal, B. Brumfield, N. LaHaye, K. Hartig and M. Phillips, *Applied Physics Reviews*, 2018, **5**, 021301.
- 14 B. T. Manard, E. M. Wylie and S. P. Willson, *Applied Spectroscopy*, 2018, **72**, 1653–1660.
- 15 A. Rao, *MSc thesis*, Air Force Institute of Technology, 2020.
- 16 A. Rao, J. Auxier, D. Vu and M. Shattan, *Laser Applications to Chemical, Security and Environmental Analysis*, 2020, p. LM1A.2.
- 17 A. P. Rao, P. R. Jenkins, J. D. Auxier II and M. B. Shattan, *J. Anal. At. Spectrom.*, 2021, **36**, 399–406.
- 18 J. L. Stakebake, *doi:10.2172/5156223*, 1992.
- 19 A. P. Rao, P. R. Jenkins, J. D. Auxier, M. B. Shattan and A. K. Patnaik, *Applied Optics*, 2022, **61**, D30–D38.
- 20 A. W. Miziolek, V. Palleschi and I. Schechter, *Laser induced breakdown spectroscopy*, Cambridge university press, 2006.
- 21 D. A. Cremers, F.-Y. Yueh, J. P. Singh and H. Zhang, *Encyclopedia of Analytical Chemistry: Applications, Theory and Instrumentation*, 2006.
- 22 A. K. Patnaik, Y. Wu, P. S. Hsu, M. Gragston, Z. Zhang, J. R. Gord and S. Roy, *Opt. Express*, 2018, **26**, 25750–25760.
- 23 A. P. Rao, M. Gragston, A. K. Patnaik, P. S. Hsu and M. B. Shattan, *Opt. Express*, 2019, **27**, 33779–33788.
- 24 J.-M. Li, L.-B. Guo, C.-M. Li, N. Zhao, X.-Y. Yang, Z.-Q. Hao, X.-Y. Li, X.-Y. Zeng and Y.-F. Lu, *Optics letters*, 2015, **40**, 5224–5226.
- 25 R. D. Cowan and G. H. Dieke, *Reviews of Modern Physics*, 1948, **20**, 418.
- 26 F. Rezaei, G. Cristoforetti, E. Tognoni, S. Legnaioli, V. Palleschi and A. Safi, *Spectrochimica Acta Part B: Atomic Spectroscopy*, 2020, **169**, 105878.
- 27 I. Karnadi, M. Pardede, I. Tanra, R. Hedwig, A. M. Marpaung, Z. S. Lie, E. Jobiliong, D. Kwaria, M. M. Suliyanti, M. Ramli et al., *Scientific reports*, 2020, **10**, 1–9.
- 28 H. Amamou, A. Bois, B. Ferhat, R. Redon, B. Rossetto and M. Ripert, *Journal of Quantitative Spectroscopy and Radiative Transfer*, 2003, **77**, 365–372.
- 29 H. Jiajia, L. Zhang, Z. Yang, W. Zhe, Y. Zhang, M. Weiguang, D. Lei, Y. Wangbao, X. Liantuan and J. Suotang, *Plasma Science and Technology*, 2019, **21**, 034016.
- 30 Z. Xiong, Z. Hao, X. Li and X. Zeng, *J. Anal. At. Spectrom.*, 2019, **34**, 1606–1610.
- 31 F. Rezaei, P. Karimi and S. H. Tavassoli, *Applied Physics B*, 2013, **114**,.
- 32 A. N. Kadachi, M. A. Al-Eshaikh and K. Ahmad, *Laser Physics*, 2018, **28**, 095701.
- 33 A. M. E. Sherbini, T. E. Sherbini, H. Hegazy, G. Cristoforetti, S. Legnaioli, L. Pardini, V. Palleschi, A. Salvetti and E. Tognoni, *Spectroscopy Letters*, 2007, **40**, 643–658.
- 34 Z. Ramezani, S. M. R. Darbani and A. E. Majd, *Appl. Opt.*, 2017, **56**, 6917–6922.
- 35 A. P. Rao, P. R. Jenkins, J. D. Auxier, M. B. Shattan and A. K. Patnaik, *J. Anal. At. Spectrom.*, 2022, **37**, 1090 – 1098.
- 36 G. Schulze, A. Jirasek, M. M. L. Yu, A. Lim, R. F. B. Turner and M. W. Blades, *Appl. Spectrosc.*, 2005, **59**, 545–574.
- 37 W. H. Press, B. P. Flannery, S. A. Teukolsky and W. T. Vetterling, *Numerical Recipes in C: The Art of Scientific Computing*, Cambridge University Press, 2nd edn, 1992.
- 38 G. F. Knoll, *Radiation detection and measurement / Glenn F. Knoll*, Wiley New York, 2nd edn, 1989, pp. xix, 754 p. .:
- 39 H. Yage, X. Wang, G. Shuai, A. Li, X. Xu, N. Wazir, D. Chunjie, T. Lu, L. Xie, M. Zhang, Y. Hao, W. Guo and R. Liu, *Applied Optics*, 2019, **58**, 422.
- 40 Y. Tang, S. Ma, Y. Chu, T. Wu, Y. Ma, Z. Hu, L. Guo, X. Zeng, J. Duan and Y. Lu, *Opt. Express*, 2019, **27**, 4261–4270.
- 41 A. Taleb, V. Motto-Ros, M. Carru, E. Axente, V. Craciun, F. Pelascini and J. Hermann, *Analytica Chimica Acta*, 2021, **1185**, 339070.
- 42 H. Hu, X. Wang and H. Zhai, *Journal of Physics D: Applied*

1            *Physics*, 2011, **44**, 135202.

2            43 M. R. Zaghloul and A. N. Ali, *ACM Transactions on Mathemat-*  
3            *ical Software (TOMS)*, 2012, **38**, 1–22.

4            44 H. R. Griem, *Principles of plasma spectroscopy*, 2005.

5            45 A. El Sherbini, T. M. El Sherbini, H. Hegazy, G. Cristo-  
6            foretti, S. Legnaioli, V. Palleschi, L. Pardini, A. Salvetti and

E. Tognoni, *Spectrochimica Acta Part B: Atomic Spectroscopy*,  
2005, **60**, 1573–1579.

46 A. de Myttenaere, B. Golden, B. L. Grand and F. Rossi, *Neuro-*  
*computing*, 2016, **192**, 38–48.

47 G. Long and J. Winefordner, *Analytical Chemistry - ANAL*  
*CHEM*, 2008, **55**,.